



# DsrA Modulates Central Carbon Metabolism and Redox Balance by Directly Repressing *pflB* Expression in *Salmonella* Typhimurium

Rui Dong,<sup>a</sup> Yuan Liang,<sup>a</sup>  Shoukui He,<sup>a</sup> Yan Cui,<sup>a</sup> Chunlei Shi,<sup>a</sup> Yiping He,<sup>b</sup>  Xianming Shi<sup>a</sup>

<sup>a</sup>MOST-USDA Joint Research Center for Food Safety, School of Agriculture and Biology, State Key Laboratory of Microbial Metabolism, Shanghai Jiao Tong University, Shanghai, China

<sup>b</sup>United States Department of Agriculture, Agricultural Research Service, Eastern Regional Research Center, Wyndmoor, Pennsylvania, USA

**ABSTRACT** Bacterial small RNAs (sRNAs) function as vital regulators in response to various environmental stresses by base pairing with target mRNAs. The sRNA DsrA, an important posttranscriptional regulator, has been reported to play a crucial role in defense against oxidative stress in *Salmonella enterica* serovar Typhimurium, but its regulatory mechanism remains unclear. The transcriptome sequencing (RNA-seq) results in this study showed that the genes involved in glycolysis, pyruvate metabolism, the tricarboxylic acid (TCA) cycle, and NADH-dependent respiration exhibited significantly different expression patterns between *S. Typhimurium* wild type (WT) and the *dsrA* deletion mutant ( $\Delta dsrA$  strain) before and after H<sub>2</sub>O<sub>2</sub> treatment. This indicated the importance of DsrA in regulating central carbon metabolism (CCM) and NAD(H) homeostasis of *S. Typhimurium*. To reveal the direct target of DsrA action, fusion proteins of six candidate genes (*acnA*, *srIE*, *tdcB*, *nuoH*, *katG*, and *pflB*) with green fluorescent protein (GFP) were constructed, and the fluorescence analysis showed that the expression of *pflB* encoding pyruvate-formate lyase was repressed by DsrA. Furthermore, site-directed mutagenesis and RNase E-dependent experiments showed that the direct base pairing of DsrA with *pflB* mRNA could recruit RNase E to degrade *pflB* mRNA and reduce the stability of *pflB* mRNA. In addition, the NAD<sup>+</sup>/NADH ratio in WT-*pflB*-*pdsrA* was significantly lower than that in WT-*pflB*, suggesting that the repression of *pflB* by DsrA could contribute greatly to the redox balance in *S. Typhimurium*. Taken together, a novel target of DsrA was identified, and its regulatory role was clarified, which demonstrated that DsrA could modulate CCM and redox balance by directly repressing *pflB* expression in *S. Typhimurium*.

**IMPORTANCE** Small RNA DsrA plays an important role in defending against oxidative stress in bacteria. In this study, we identified a novel target (*pflB*, encoding pyruvate-formate lyase) of DsrA and demonstrated its potential regulatory mechanism in *S. Typhimurium* by transcriptome analysis. *In silico* prediction revealed a direct base pairing between DsrA and *pflB* mRNA, which was confirmed in site-directed mutagenesis experiments. The interaction of DsrA-*pflB* mRNA could greatly contribute to the regulation of central carbon metabolism and intracellular redox balance in *S. Typhimurium*. These findings provided a better understanding of the critical roles of small RNA in central metabolism and stress responses in foodborne pathogens.

**KEYWORDS** DsrA, central carbon metabolism, sRNA, oxidative stress resistance, *pflB*, *Salmonella*

*Salmonella* is a Gram-negative, facultative anaerobe and generalist pathogen that is capable of causing bacteremia, gastroenteritis, and systemic infection in a range of different hosts (1). During its infectious cycle, *Salmonella* is recognized by macrophages, neutrophils,

**Editor** Amanda G. Oglesby, University of Maryland School of Pharmacy

This is a work of the U.S. Government and is not subject to copyright protection in the United States. Foreign copyrights may apply.

Address correspondence to Xianming Shi, xmshi@sjtu.edu.cn.

The authors declare no conflict of interest.

**Received** 10 September 2021

**Accepted** 3 January 2022

**Published** 2 February 2022

and dendritic cells, all of which internalize and comprise the bacterium in a *Salmonella*-containing vacuole (SCV), where *Salmonella* faces several stresses, including imbalanced reactive oxygen/nitrogen species (ROS/RNS), low pH, and iron deficiency (2, 3).

Oxidative stress response is essential to microbial adaptability and pathogenicity (4). An elaborate ROS defense system enables bacteria to survive in a multitude of environmental stresses (5). These defense mechanisms include scavenging enzymes involved in detoxification of reactive radicals and repair enzymes used for restoring cellular physiology (6, 7). NADH, generated primarily in the tricarboxylic acid (TCA) cycle, plays an important role in cell synthesis and detoxifying ROS. Conversely, NADH is the source of energy generation in the respiratory chain reactions, which produce ROS. Thus, bacteria need to redistribute the flux of central carbon metabolism (CCM) to rebalance redox reaction by modulating the multilevel regulation machinery (8). For instance, CCM could generate more reduced equivalent (NADH) to reduce oxidative stress by modulating the fluxes (8). Also, many enzymes involved in CCM, such as succinate dehydrogenase (Sdh), fumarate reductase (Frd), and aconitase (Acn), contain flavins or iron-sulfur clusters for univalent redox reactions (7, 9). Without this protection, a number of crucial cellular components in *Salmonella*, including DNA, RNA, proteins, and membrane lipids, would be structurally or functionally deterred from augmentation of ROS (10–12).

Small RNAs (sRNAs) have significant effects on gene expression by reinforcing transcriptional regulation and providing links between different regulatory modules (13). Bacterial sRNAs have been reported to play an important role in response to various environmental stresses, such as, carbon starvation (14), virulence (15, 16), acid stress (17), oxidative stress (18, 19), and antibiotics (20, 21). Since most sRNAs bind to their mRNA targets by imperfect complementarity, they are often found to regulate multiple genes and rewire complex regulatory networks (13, 22). However, even with multiple validated targets, sRNA usually has much more target candidates based on prediction. These candidates, under given conditions, are found not to interact with the sRNA directly (23, 24). This raises the notion that some of them could be regulated by the sRNA under alternative conditions.

In our previous work, DsrA was found to play an important role in oxidative stress resistance of *Salmonella enterica* serovar Typhimurium (25). However, the regulatory mechanism of DsrA in defending against oxidative stress remains unclear. To reveal the target of DsrA action, in this study, we performed a whole-genome transcriptome analysis, characterized the *in silico* predicted DsrA targets, and investigated the direct interaction between DsrA and its targets by site-directed mutagenesis.

## RESULTS

**Overview of RNA-seq.** In pursuit of the biological role of DsrA, gene expression before and after a 30-min H<sub>2</sub>O<sub>2</sub> treatment was compared in the  $\Delta dsrA$  strain and in the WT as well. Among 12 samples, a range of 4,042 to 4,119 genes per sample were detected, which accounted for 71.8% to 73.3% of the whole genome (5,623 genes) in *S. Typhimurium*. In the H<sub>2</sub>O<sub>2</sub>-treated WT compared to an untreated sample, 1,389 genes were significantly ( $P < 0.05$ ) differentially expressed, including 597 upregulated genes and 792 downregulated genes (Fig. 1A). In the  $\Delta dsrA$  strain after the treatment, 530 and 586 genes were significantly ( $P < 0.05$ ) up- and downregulated, respectively (Fig. 1B).

Comparative analysis of differentially expressed genes (DEGs) in the WT and  $\Delta dsrA$  strain was shown in Fig. 1C. It was found that seven genes (*srlA*, *srlE*, *slrB*, *tdcB*, *nrdD*, *treC*, and *sdaC*) were downregulated in WT while upregulated in the  $\Delta dsrA$  strain, and an additional 346 genes were exclusively downregulated in WT but showed no apparent changes in the  $\Delta dsrA$  strain, suggesting that DsrA might negatively regulate the expression of these genes. However, two genes (*ypeC* and *clpA*) were upregulated in WT but downregulated in the  $\Delta dsrA$  strain, and 276 genes were exclusively upregulated in WT while not changed in the  $\Delta dsrA$  strain, suggesting that DsrA might positively regulate the expression of this set of genes.

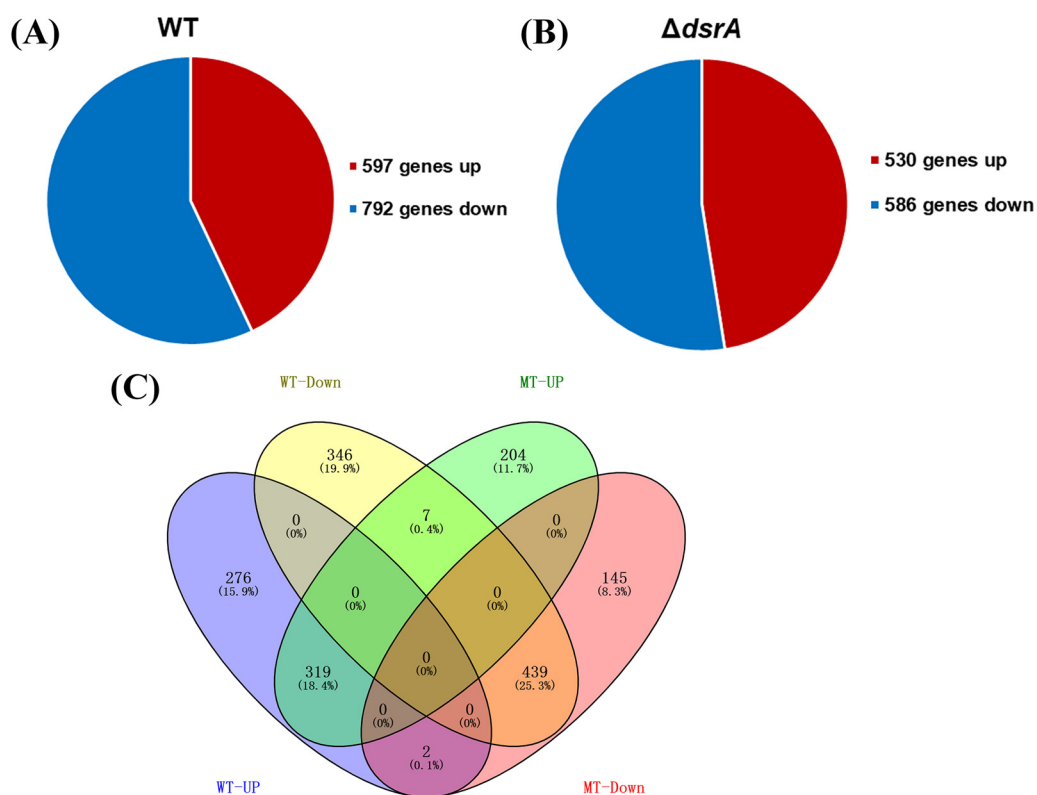


**FIG 1** Overview of RNA-seq. (A) Pie graph of DEGs in wild type. (B) Pie graph of DEGs in the  $\Delta dsrA$  strain. (C) Venn diagram showing DEGs in wild type (WT) and the  $\Delta dsrA$  strain (MT). Genes with a fold change of  $\geq 2$  and Bonferroni-corrected  $P$  value ( $P_{adj}$ ) of  $< 0.05$  were determined to be DEGs.

The DEGs were also subjected to functional categorization using the KEGG database (see Fig. S1 in the supplemental material). It was found that there were more upregulated and less downregulated genes in both the carbohydrate metabolism pathway and global metabolism pathway in the  $\Delta dsrA$  strain than those in WT (Fig. S1). The differences of DEG profile in these pathways between WT and mutant suggested DsrA might have a nonnegligible role in metabolic regulation in *S. Typhimurium*.

**Validation of RNA-seq data via RT-qPCR.** The  $H_2O_2$ -induced changes in transcript expression were validated by quantitative real-time PCR (RT-qPCR). A number of representative genes were randomly selected from the differentially expressed genes identified in transcriptome sequencing (RNA-seq). In WT, six genes (*iroB*, *sufA*, *soxR*, *dps*, *ahpF*, and *katG*) with increased transcript abundances and four genes (*nuoH*, *srlA*, *bssR*, and *tdcB*) with decreased transcript abundances were selected for RT-qPCR analysis. In the  $\Delta dsrA$  strain, 10 differentially transcribed genes, including six upregulated (*sufA*, *soxR*, *dps*, *srlA*, *tdcB*, and *ahpF*) and four downregulated (*cadA*, *lamB*, *bssR*, and *pduA*) genes were selected for the same purpose. The RT-qPCR results showed a good correlation with the RNA-seq data in both WT ( $R^2 = 0.997$ ,  $P < 0.0001$ ) and the  $\Delta dsrA$  strain ( $R^2 = 0.979$ ,  $P < 0.0001$ ) (Fig. 2), supporting the reliability and validity of the RNA-seq data.

**Regulatory effect of DsrA on central carbon metabolism.** The expression of the genes related to NAD-dependent oxidation in CCM, including glycolysis, tricarboxylic acid (TCA) cycle, and pyruvate metabolism, was analyzed in this study. Figure 3A shows the genes with  $H_2O_2$ -altered transcript expression in the  $\Delta dsrA$  strain or WT involved in glycolysis. After  $H_2O_2$  treatment, the pyruvate kinase gene (*pykA*) was downregulated (2.15-fold) in WT but slightly upregulated (1.31-fold) in the  $\Delta dsrA$  strain. Another pyruvate kinase gene (*pykF*) was transcribed higher in both WT (2.82-fold) and the  $\Delta dsrA$  strain (6.84-fold) after  $H_2O_2$  treatment, whereas upregulated magnitude was substantial in the  $\Delta dsrA$  strain (Fig. 3A). The *ackA-pta* operon, which converts acetyl coenzyme A (acetyl-CoA) to acetate (Fig. 4), was upregulated in WT (3.31-fold) but not changed in

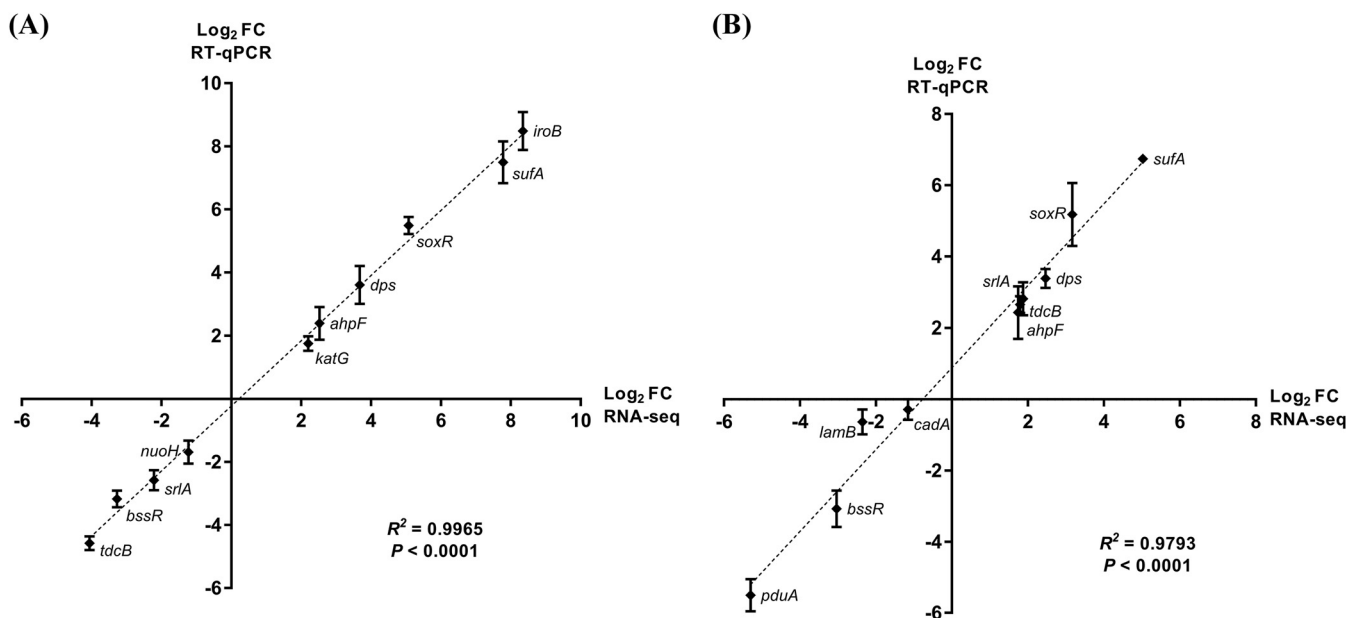


**FIG 2** RT-qPCR validation of RNA-seq data for selected differentially expressed genes. The relative transcription of genes found to be differentially regulated in the RNA-seq analysis of the wild-type strain (A) or  $\Delta dsrA$  strain (B) after  $H_2O_2$  treatment was examined by RT-qPCR. 16S rRNA was used as a reference gene. Mean  $\log_2$  fold change (FC) in the transcription of genes in six independent RT-qPCR experiments were plotted against the respective  $\log_2$  FC determined by RNA-seq. The coefficient of determination ( $R^2$ ) and  $P$  value were calculated in Microsoft Excel.

the  $\Delta dsrA$  strain. Similar to *pykF*, *adhE* encoding alcohol dehydrogenase was expressed higher in both WT (2.43-fold) and the  $\Delta dsrA$  strain (4.58-fold) after  $H_2O_2$  treatment (Fig. 4). The upregulated magnitude in the  $\Delta dsrA$  strain was more significant.

Our results showed that the expressions of *aceE*, *aceF*, *pdhR*, and *lpdA*, which were involved in pyruvate metabolism (Fig. 4), were significantly upregulated in both WT (19.45-, 17.93-, 11.91-, and 2.02-fold, respectively) and the  $\Delta dsrA$  strain (15.32-, 10.02-, 2.34-, and 2.70-fold, respectively) after  $H_2O_2$  treatment, indicating pyruvate was actively metabolized under oxidative stress (Fig. 3B). The expression of *pflB* was downregulated (2.72-fold) in WT while slightly upregulated (1.49-fold) in the  $\Delta dsrA$  strain after  $H_2O_2$  treatment (see Fig. 3B and Fig. 6A). In contrast to *pflB*, the expression of *ldhA* was significantly increased (5.32-fold) in WT and slightly decreased (1.43-fold) in the  $\Delta dsrA$  strain after the treatment, suggesting the coupling between NADH production and consumption in the pyruvate-to-lactate and pyruvate-to-formate reactions (Fig. 4).

Under  $H_2O_2$  treatment, the TCA cycle activity was generally repressed in WT, while the genes involved in the TCA cycle showed different trends of expression in the  $\Delta dsrA$  strain (Fig. 3C). Notably, *acnA* encoding aconitate hydratase (Fig. 4), which is involved in oxidative stress response, showed a significantly high expression (3.72-fold) in WT but minor change in the  $\Delta dsrA$  strain. In addition, the isocitrate dehydrogenase gene (*icdA*) expressed slightly higher (1.13-fold) in WT and lower (1.45-fold) in the  $\Delta dsrA$  strain. The expression of *sucB* encoding  $\alpha$ -ketoglutarate dehydrogenase was not changed in WT but significantly increased (2.54-fold) in the  $\Delta dsrA$  strain (Fig. 4). Intriguingly, *sucC* (3.01-fold) and *sucD* (2.99-fold) showed a similar expression pattern to *sucB*, most likely because *sucCD* and *sucB* are in the same operon (Fig. 4).

**Regulatory effect of DsrA on cell respiration.** NADH generated from the TCA cycle can be oxidized by NADH dehydrogenase (NDH) in the respiratory chain reactions (Fig. 4). The expression of genes encoding NDH was analyzed in this study. The *ndh* gene encoding NDH-2 showed an increasing expression both in WT (7.2-fold) and the  $\Delta dsrA$  strain (6.17-fold). In addition, the entire *nuo* operon encoding NDH-1 was downregulated in WT after  $H_2O_2$  treatment, of which *nuoHIJKLMN* had a significantly lower expression (Fig. 3D). Despite sharing the same operon, the *nuo* operon in the  $\Delta dsrA$  strain showed different expression patterns with slightly decreased *nuoABC* but increased *nuoE-nuoN* transcripts after  $H_2O_2$  treatment (Fig. 3D).

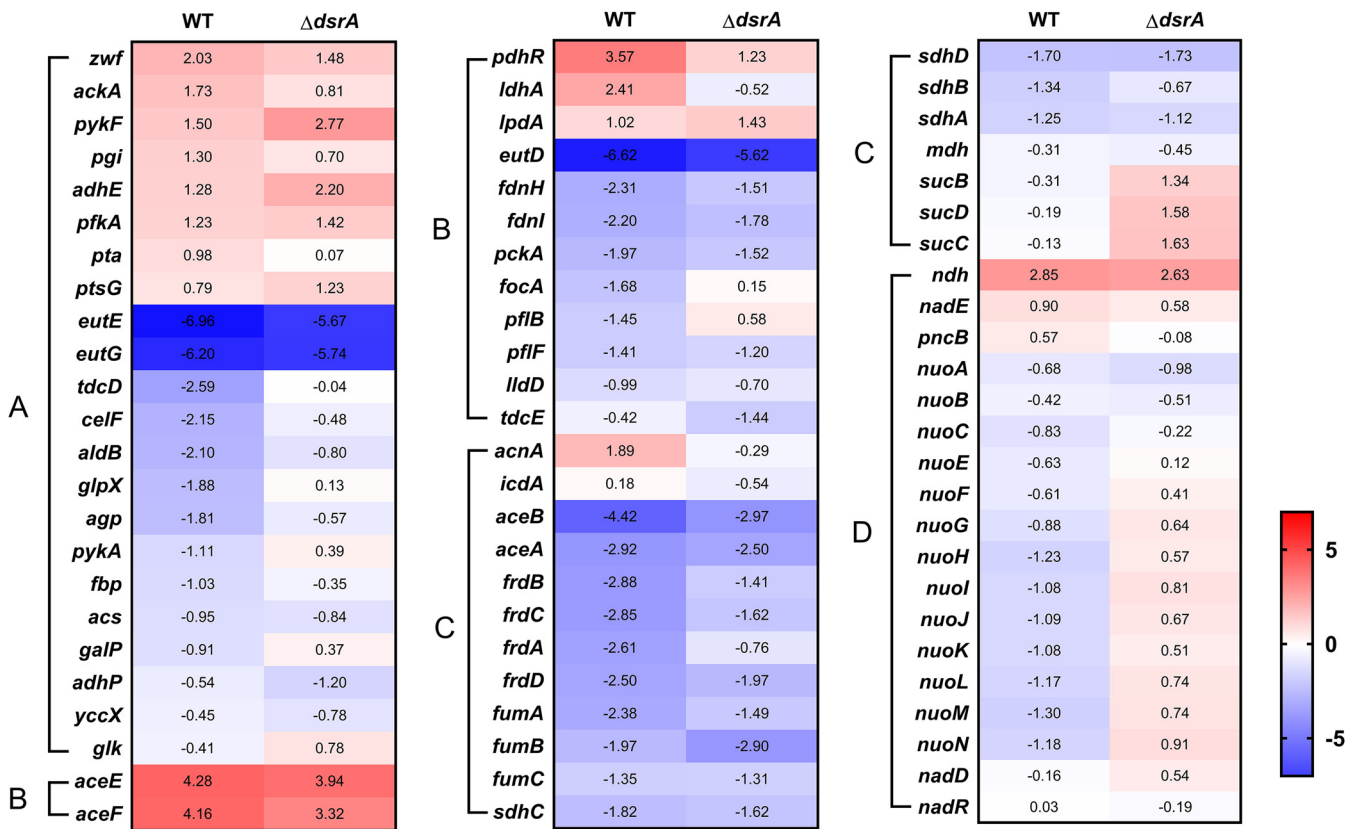


**FIG 3** Heat map of genes involved in the major metabolic pathways in the wild-type and  $\Delta dsrA$  strains after  $H_2O_2$  treatment. (A) Glycolysis. (B) Pyruvate metabolism. (C) TCA cycle. (D) NADH-dependent respiration. Each row represents an individual gene.  $\log_2$  FC of genes were labeled in the corresponding grid. The scale of this heat map is given as  $\log_2$  FC ranging from  $-7$  (blue) to  $+7$  (red).

**Predicted mRNA targets of DsrA in *S. Typhimurium*.** To find out the target of DsrA, comparative analysis of the whole-genome expression in WT and the  $\Delta dsrA$  strain was performed, and *in silico* prediction was run in the CopraRNA and IntaRNA webserver (26). Six predicted genes (*acnA*, *srlE*, *tdcB*, *nuoH*, *katG*, and *pflB*) were selected as target candidates based upon the output of the query. For preliminary evaluation of the predictions, expressions of the candidate genes in the presence and absence of DsrA were compared by RT-qPCR analysis. As shown in Fig. 5A, the mRNA levels of *pflB*, *nuoH*, *srlE*, and *tdcB* were significantly higher in the  $\Delta dsrA$  strain or  $\Delta dsrA$ -pZE0 strain than those in WT or the  $\Delta dsrA$ -pdsrA strain, suggesting the negative regulatory effect of DsrA on the four genes. On the contrary, the expression of *acnA* and *katG* in the  $\Delta dsrA$  strain or  $\Delta dsrA$ -pZE0 strain was significantly lower than that in WT or the  $\Delta dsrA$ -pdsrA strain, indicating the positive regulation of DsrA on these two genes.

To further evaluate the prediction results, six target gene fusions were constructed by using an established two-plasmid reporter system as previously described (27, 28), in which DsrA was expressed in the pZE12-*luc* plasmid and a predicted mRNA target was expressed as an sfGFP-fusion protein in the pXG reporter plasmid. pZE0 expressing a 10-nt nonsense nucleotide and pXG1 were used as the negative control plasmids for sRNA expression and mRNA target expression fusion, respectively. The fusion of *hns::gfp* was also constructed in parallel as the positive control since *hns* is a well-known target repressed by DsrA (28). Of the six genes tested, the fluorescence of *pflB::gfp* in the  $\Delta dsrA$ -pdsrA strain was significantly lower than that in the  $\Delta dsrA$ -pZE0 strain, indicating that DsrA could repress the expression of *pflB* (Fig. 5B).

**Evidence for DsrA-*pflB* mRNA interaction by direct base pairing.** Based on *in silico* prediction, DsrA can base pair with the mRNA sequence of *pflB* to form a 12-bp RNA-RNA duplex (Fig. 6A and C). This base pairing was experimentally confirmed by mutating the nucleotide sequences in DsrA and *pflB::gfp* to disrupt the pairing and by

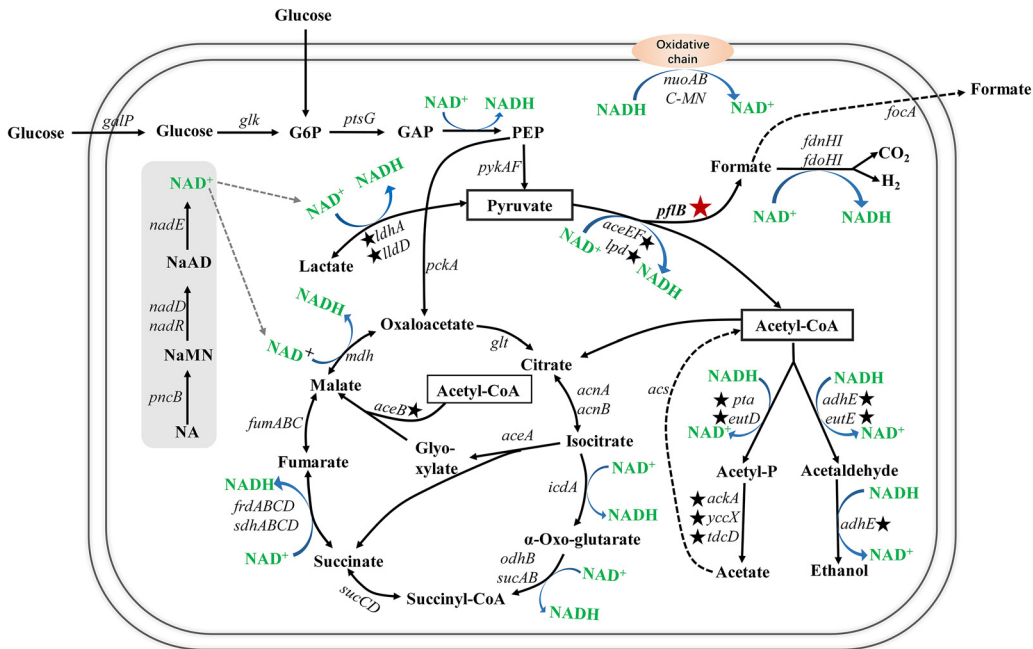


**FIG 4** Biochemical pathways involved in NAD(H) cycle in *S. Typhimurium*. The red star represents the verified target of DsrA in this study. Black stars represent the predicted proteins that could interact with PflB.

compensating these mutations to restore the pairing (Fig. 6C). Overexpression of a mutant variant of DsrA (*pdsrA\**) carrying 2-nucleotide substitutions in the predicted base-pairing region resulted in failure to repress the expression of wild-type *pflB::gfp* fusion (Fig. 6D). Consistently, introducing a compensatory mutation in the *pflB::gfp* (*pflB\**) by a mutation completely abolished the repression by wild-type DsrA. However, the compensatory mutation was efficiently suppressed by overexpression of *pdsrA\** (Fig. 6D). Taken together, these results suggested that translational repression of *pflB* by DsrA was mediated by direct base pairing.

**The repression effect of DsrA on *pflB* was RNase E dependent.** Alignment of *pflB* gene sequences revealed its high conservation among various *Salmonella* species (Fig. 6A). Notably, the sequence AAATT around the DsrA-*pflB* mRNA interaction site matched a consensus motif for RNase E in *Salmonella* (RN↓WUU) (Fig. 6A) (29). As a result, we then checked whether DsrA affected *pflB* mRNA in an RNase E-dependent manner using a thermosensitive RNase E mutant (*rne-Ts*) (30, 31). The *dsrA* deletion mutant ( $\Delta dsrA$  strain), *dsrA* wild-type expression strain ( $\Delta dsrA$ -*pdsrA* strain), and *dsrA* site mutant expression strain ( $\Delta dsrA$ -*pdsrA\** strain) of *rne-Ctr* strain and *rne-Ts* strain were constructed, respectively, and the expressions of *pflB* in different strains were analyzed. As shown in Fig. 6F, the negative regulatory effect of DsrA on *pflB* was found in the *rne-Ctr* strain; however, it was abrogated in the *rne-Ts* strain at 44°C where RNase E was inactivated. Intriguingly, there were no significant differences in *pflB* expression between the  $\Delta dsrA$ -*pdsrA* and  $\Delta dsrA$ -*pdsrA\** strains of the *rne-Ctr* strain at 44°C.

In order to be consistent with the RNA-seq condition, the *pflB* expression analyses in the *rne-Ctr* strain and *rne-Ts* strain was also performed under 37°C, where we thought that RNase E activity might be partially inhibited. As shown in Fig. 6E, *pflB* expression in the Ctr- $\Delta dsrA$  or Ctr- $\Delta dsrA$ -pZE0 strains was prominently higher than that in the Ctr-WT or Ctr- $\Delta dsrA$ -*pdsrA* strain. In addition, the *pflB* expression in the Ctr- $\Delta dsrA$ -*pdsrA\** strain was also significantly higher than that in the Ctr- $\Delta dsrA$ -*pdsrA* strain, which indicated DsrA could directly repress the expression of *pflB* in the presence of RNase E. However, *pflB* expression showed no considerable differences among the Ts- $\Delta dsrA$ , Ts- $\Delta dsrA$ -pZE0, Ts- $\Delta dsrA$ -*pdsrA*, and Ts- $\Delta dsrA$ -*pdsrA\** strains. These results suggested that the repression effect of DsrA on *pflB* was RNase E dependent. The base-

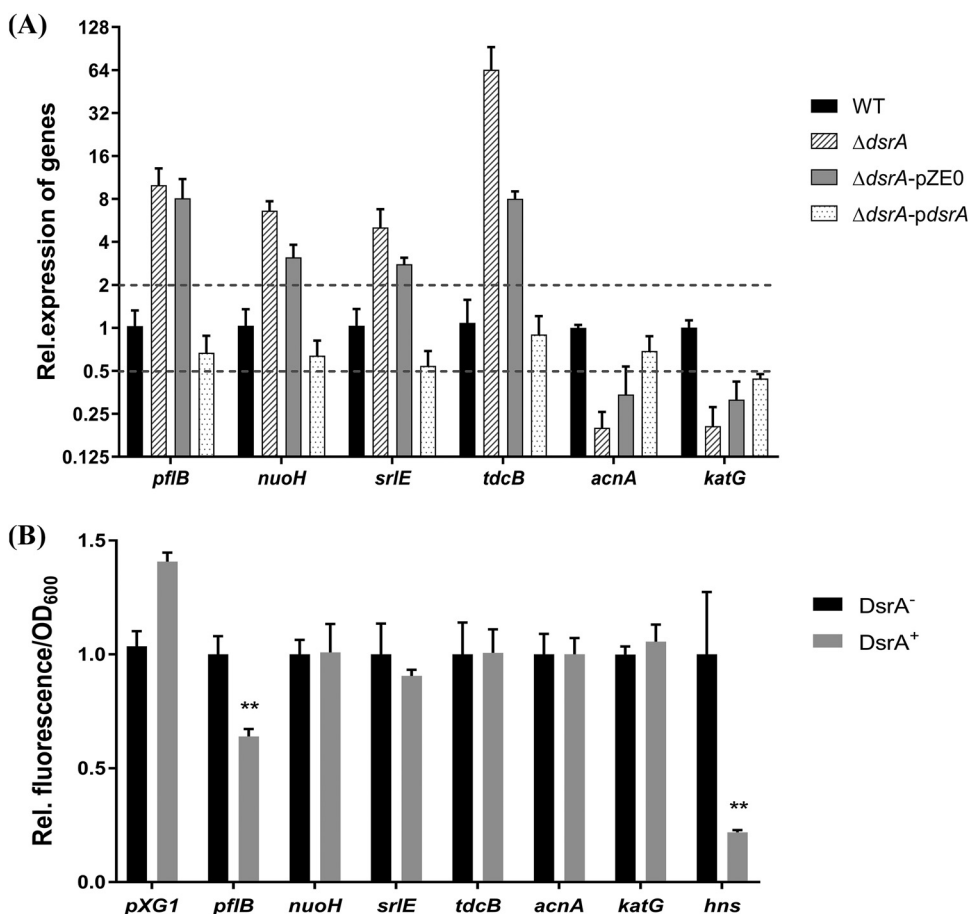


**FIG 5** The regulatory effect of DsrA on six target candidates. (A) The relative expression of *pflB*, *nuoH*, *srlE*, *tdcB*, *acnA*, and *katG* in the wild-type,  $\Delta dsrA$ ,  $\Delta dsrA$ -pZE0, and  $\Delta dsrA$ -pdsrA strains was determined by RT-qPCR. 16S rRNA was used as a reference gene. The expression of genes in the wild type was regarded as 1. (B) Fluorescence measurement of target expression fusion with GFP. The 5' UTRs or intergenic regions of candidate target mRNAs were cloned into pXG-10sf or pXG-30sf vectors, respectively. GFP expression in the LB liquid medium was quantified by a microplate reader and normalized by OD<sub>600</sub>. pZE0 and pXG1 were used as negative control plasmids for DsrA expression and target gene fusion plasmid, respectively. *hns::gfp* was constructed as the positive control for DsrA regulation. \*\*,  $P < 0.01$

pairing of DsrA might recruit RNase E to degrade *pflB* mRNA and reduce the stability of *pflB* mRNA.

**Effect of the repression of *pflB* by DsrA on the redox balance in *Salmonella*.** To evaluate the physiological effect of DsrA on *pflB*, a *pflB*-overexpression strain (WT-*ppflB*) and a *pflB*-*dsrA* cooverexpression strain (WT-*ppflB*-*pdsrA*) were constructed. The plasmid pHM1 was used as the negative control plasmid for *pflB* expression. The NAD<sup>+</sup>/NADH ratio was measured in the WT,  $\Delta dsrA$ ,  $\Delta dsrA$ -pZE0,  $\Delta dsrA$ -pdsrA, WT-pHM1, WT-*ppflB*, and WT-*ppflB*-*pdsrA* strains. As shown in Fig. 7A, both the  $\Delta dsrA$  and  $\Delta dsrA$ -pZE0 strains exhibited a considerably higher NAD<sup>+</sup>/NADH ratio than WT, with a more marked effect in the presence of H<sub>2</sub>O<sub>2</sub>, suggesting that the redox balance could be altered in the  $\Delta dsrA$  strain and severely perturbed under oxidative stress. Likewise, the NAD<sup>+</sup>/NADH ratio was significantly higher in the WT-*ppflB* strain than that in WT or WT-pHM1, regardless of the presence or absence of H<sub>2</sub>O<sub>2</sub>, indicating the redox imbalance in the WT-*ppflB* strain. It was found that PflB could interact with several proteins related to NAD-dependent reaction, which echoed the role of *pflB* in disturbed redox balance (Fig. 7B). However, the WT-*ppflB*-*pdsrA* strain showed a significantly lower NAD<sup>+</sup>/NADH ratio than the WT-*ppflB* strain, indicating that overexpression of DsrA could prominently improve the redox balance in the WT-*ppflB* strain. Taken together,

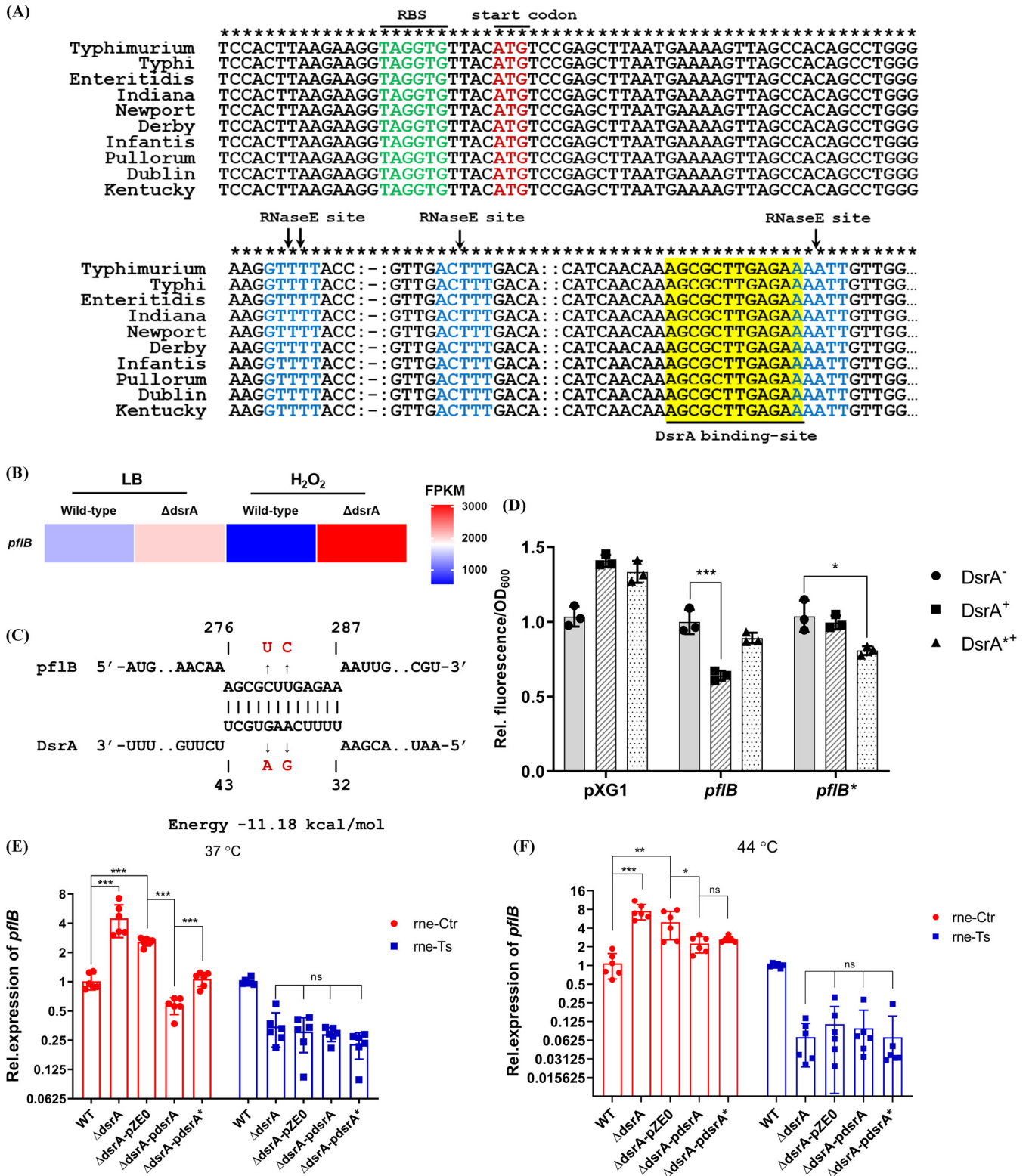


**FIG 6** The regulatory effect of DsrA on *pf1B*. (A) Alignment of *pf1B* gene from various *Salmonella* species. Asterisks indicate the conserved nucleotides. The RBS region was marked in green. The start codon was marked in red. The RNase E sites were marked in blue. The DsrA-*pf1B* interaction regions were highlighted. The symbol “-:” indicates a 165-bp insertion. The symbol “::” indicates a 40-bp insertion. (B) Heat map of *pf1B* expression in the wild type and  $\Delta dsrA$  strains before and after H<sub>2</sub>O<sub>2</sub> treatment. (C) Predicted interactions of *Salmonella* DsrA with *pf1B* mRNA. Mutated nucleotides were indicated by red letters. The numbers represented the position of nucleotides in the *pf1B* CDS region from start codon or DsrA RNA from transcription start site. (D) DsrA regulates the *pf1B* mRNA by base pairing mechanism. The  $\Delta dsrA$  strain was transformed by combinations of pXG plasmids along with control plasmid (pZEO), DsrA expression plasmid (*pdsrA*), or the DsrA mutant expression plasmid (*pdsrA*<sup>\*</sup>) as indicated. GFP expression in the LB liquid medium was

(Continued on next page)



conversion of acetyl-CoA to ethanol coupled with the production of oxidative equivalent  $\text{NAD}^+$ , both of which were not conducive to the  $\Delta dsrA$  strain in defense against oxidative stress.

The TCA cycle is usually repressed under oxidative stress to increase the formation of  $\alpha$ -ketoglutarate (37, 38).  $\alpha$ -Ketoglutarate is another ketoacid that can relieve oxidative stress by nonenzymatic reactions (35). The expression patterns of *icdA* and *sucB* genes found here suggested an accumulation of  $\alpha$ -ketoglutarate in WT and a degradation of  $\alpha$ -ketoglutarate in the  $\Delta dsrA$  strain under oxidative stress, which would lead to less resistance to oxidative stress in the  $\Delta dsrA$  strain than in the WT.

**Broad spectrum of DsrA-target interaction.** Similar to transcriptional factors, sRNA can simultaneously target multiple mRNAs (39). It was reported that *Escherichia coli* could express approximately 300 sRNAs and develop over 2,000 unique sRNA-mRNA target interactions (40–42). *Salmonella* is also able to express approximately 300 sRNAs (42, 43), which implies that *Salmonella* might also harbor a complex network of sRNA-mRNA interactions. The secondary structure of DsrA contains three stem loops, denoted as SL1, SL2, and SL3, and a long linker between SL1 and SL2 (44). The conformational flexibility makes DsrA more accessible to multiple mRNA binding. Currently, five targets have been determined for DsrA, namely, *rpoS*, *hns*, *mreB*, *rbsD*, and *lrp*, among which only *rbsD* is targeted in the coding DNA sequence (CDS) region far downstream of the start codon, and the other four are targeted in the region near the start codon (44–48).

Targeting the CDS region of mRNA to induce mRNA degradation is an important mechanism for small RNA regulation (49–51). Many sRNAs have been reported to function in this way, such as the *CoaR/tcpl* system, *GcvB/asnA* system, and *MicC/ompD* system (16, 50, 52). sRNA MicC binds the *ompD* mRNA far downstream of the ribosome binding site (RBS) (+67 to +78 nucleotide from the start codon) and induces RNase E cleavage at the +83 position of *ompD* mRNA in conjunction with Hfq (52). The tricompound of sRNA, Hfq, and RNase E binds the target sequence via the MicC “seed sequence,” since RNase E-mediated mRNA degradation requires specific structural features containing an A/U-rich sequence and an adjacent secondary structure (53–55). In this study, the sequence “AAATT” downstream of the DsrA-*pflB* mRNA interaction site matched a consensus motif for RNase E in *Salmonella* (RN↓WUU) (29). The DsrA-*pflB* duplex and the “AAATT” sequence provided conditions for RNase E digestion. In addition, an AAN-repeat sequence “AACAAA” was found upstream of the DsrA binding site in *pflB* mRNA, which was consistent with the distal face-binding motif of Hfq (A-A-N)<sub>n</sub> and might allow Hfq to bind the mRNA to recruit RNase (56, 57). All discussed above indicated that the binding of DsrA with *pflB* could promote the formation of the DsrA-Hfq-RNase E complex and induce the RNase E cleavage on *pflB* mRNA.

Among six target candidates in this study, only *pflB::gfp* was repressed by DsrA, which highlighted the strength and weakness of *in silico* prediction. Site-directed mutation analysis was performed to explore the interaction between DsrA and *pflB*. Intriguingly, the inhibition of *pflB* was not completely abolished by mutation of DsrA, and the regulation of *pflB*\* by DsrA\* was also just partially restored, which implied that DsrA could not only directly regulate *pflB* expression but also indirectly regulate *pflB* expression through other means (Fig. 6D and E). In addition, *pflB* expression in the Ctr- $\Delta dsrA$ -*pdsrA*\* strain was significantly higher than that in the Ctr- $\Delta dsrA$ -*pdsrA* strain at 37°C, while showing no significant differences compared with that in the Ctr- $\Delta dsrA$ -*pdsrA* strain at 44°C (Fig. 6E and F). Similarly, it was reported that most sRNA partners in RIL-seq data would not be predicted by CopraRNA, or their gene expressions were not affected when tested with reporter fusions (58), indicating that sRNAs, including DsrA, could regulate specific genes under specific conditions.

**DsrA regulated the redox balance by repressing *pflB* in *S. Typhimurium*.** *pflB* is the second gene in the *focA-pflB* operon that encodes a metabolic pathway converting pyruvate to acetyl-CoA with formate as a by-product (Fig. 4) (59). The evolution of PflB is important for bacteria to tolerate oxidative stress (7). We found that the *pflB* gene was highly conserved in various *Salmonella* species (Fig. 6A) but less conserved among

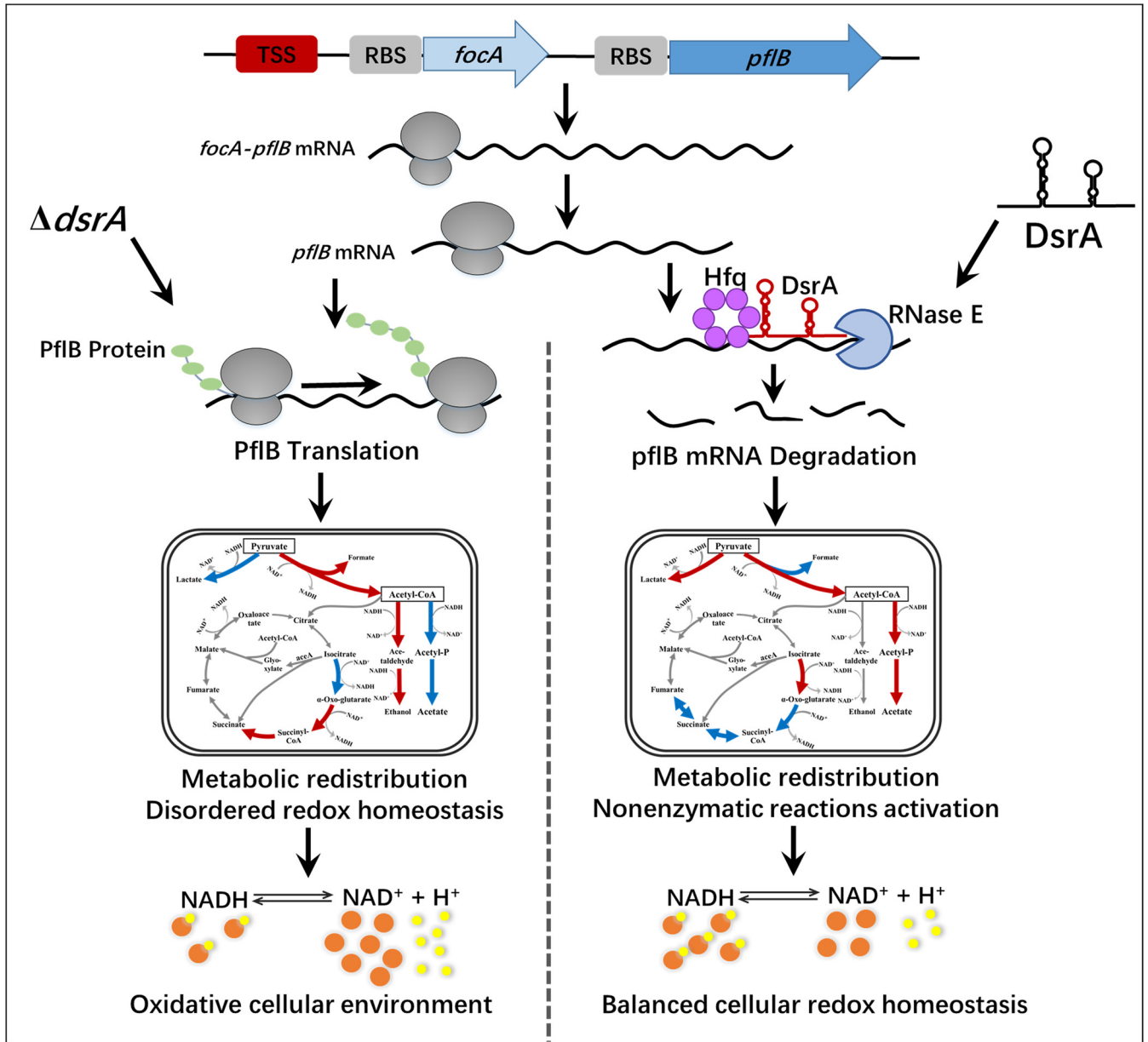


**FIG 8** Proposed model for the regulation of NAD(H) homeostasis by DsrA-pflB mRNA interaction. Red arrows represent the metabolic pathways with increased flux. Blue arrows represent the metabolic pathways with reduced flux.

different microbial species, such as *Salmonella* and *E. coli* (data not shown), which may result from the evolutionary differences among species. Consistent with our results, a double deletion mutant of *pflB* and *ldhA* in *E. coli* showed an extremely low intracellular NAD<sup>+</sup>/NADH ratio, and this NAD<sup>+</sup>/NADH imbalance was mainly caused by the inactivation of PFL rather than the inactivation of LDH (60–62), which highlighted the importance of PflB in maintaining cellular redox homeostasis.

Several proteins (i.e., LdhA, AceE, AceF, Pta, AckA, and AdhE) in pyruvate metabolism pathway were predicted by STRING software to interact with PflB (Fig. 7B). This could explain, to some extent, the difference in pyruvate metabolic flux between the WT and  $\Delta dsrA$  strains (Fig. 4 and 8). AdhE was reported to regulate the activity of pyruvate formate lyase (PFL) (63). Thus, to inhibit PflB activity in the  $\Delta dsrA$  strain, cells might activate the expression of AdhE. The high expression of AdhE would also generate excess NAD<sup>+</sup> and enhance the imbalance of redox reaction (Fig. 8). If the expression of *dsrA* was restored, the above circumstances would be improved (Fig. 8). Notably, the

increased magnitude of the  $\text{NAD}^+/\text{NADH}$  ratio in the  $\Delta dsrA$  strain compared to WT was much higher than that in the WT-*ppflB* strain (Fig. 7A), indicating the more significant effect of DsrA on redox homeostasis than *ppflB*. As an important posttranscriptional regulator, DsrA might act at the center of the regulatory network. It could simultaneously interact with multiple targets and regulate the redox balance of *S. Typhimurium* through multiple mechanisms in addition to repression of *ppflB*.

In this study, the critical role of DsrA in regulating CCM and NAD(H) homeostasis in *S. Typhimurium* was elucidated by transcriptome analysis. A novel target of DsrA, *ppflB* encoding pyruvate-formate lyase, was identified from the studies of PflB-GFP fusion proteins in the presence and absence of DsrA. Direct base pairing between DsrA and *ppflB* mRNA sequences was predicted *in silico* and confirmed by mutational analysis. Moreover, phenotype analysis of intracellular redox homeostasis showed that the interaction between DsrA-*ppflB* mRNA could greatly contribute to the redox balance in *S. Typhimurium* (Fig. 8).

## MATERIALS AND METHODS

**Bacterial strains and growth conditions.** *S. Typhimurium* strain ATCC14028 is referred to as wild type (WT) and was used for mutant construction. Bacterial cells were grown at 37°C with reciprocal shaking at 220 rpm in LB broth. Where appropriate, the medium was supplemented with antibiotics at the concentrations of 100  $\mu\text{g}/\text{mL}$  ampicillin (Amp), 34  $\mu\text{g}/\text{mL}$  chloramphenicol (Cm), 40  $\mu\text{g}/\text{mL}$  spectinomycin (Sm), and 100  $\mu\text{g}/\text{mL}$  hygromycin B (HYG).

For  $\text{H}_2\text{O}_2$  treatment, a single colony was inoculated into fresh LB broth and grown at 37°C with rotation at 200 rpm until an optical density at 600 nm ( $\text{OD}_{600}$ ) of 1.0 was achieved. Each culture was then inoculated at a dilution of 1:100 into 5 mL fresh LB and grown to mid-log phase. This was followed by the treatment of 3 mM  $\text{H}_2\text{O}_2$  for 30 min. After that, the cells were collected for subsequent experiments.

**Strain construction.** The  $\Delta dsrA$  and  $\Delta dsrA$ -*pdsrA* strains were obtained from the same source as indicated in our previous work (25). Plasmid pZE0, which expresses a 10-nt nonsense RNA, was the negative control vector for sRNA expression plasmids. All of the strains used in this study are summarized in Table 1. A complete list of plasmids and oligonucleotides is included in Tables S1 and S2 in the supplemental material.

DsrA deletion strains of *rne*-Ctr and *rne*-TS were constructed using  $\lambda$ -Red recombinase one-step inactivation method (64). Briefly, the upstream fragment of *dsrA*, HYG-resistant fragment, and the downstream fragment of *dsrA* were linked by overlapping PCR to produce the  $\Delta dsrA::hph$  fragment, followed by gel purification. Then 100 ng of  $\Delta dsrA::hph$  fragments was transformed into *Salmonella* wild-type carrying the pKD46 helper plasmid. Phage22 was used to transduce the  $\Delta dsrA::hph$  fragment to the *rne*-Ctr WT or *rne*-Ts WT strain (65). The correct insertions of the HYG marker gene were verified by PCR using *dsrA*-F1&R2.

To construct the *ppflB* overexpressing strain, the entire CDS region of *ppflB* was amplified using the primer set of *ppflB*-F&R followed by gel purification. The PCR products and pHM1 vector were digested using Sall/EcoRI. The digested products were ligated for 1 h at 22°C to generate a recombinant plasmid pHM-*ppflB*. Subsequently, pHM-*ppflB* was transferred into the WT strain and selected on Sm plates to yield the *ppflB* overexpressing strain (WT-*ppflB*). To construct the *ppflB* and *dsrA* double overexpressing strain, *ppflB* overexpressing plasmid (pHM-*ppflB*) and *dsrA* overexpressing plasmid (pZE-*dsrA*) were simultaneously transformed into WT and selected on the plates containing Amp and Sm to yield the WT-*pdsrA*-*ppflB* strain.

**RNA-seq sample preparation.** Cells of WT,  $\Delta dsrA$ , and  $\Delta dsrA$ -*pdsrA* strains before and after  $\text{H}_2\text{O}_2$  treatment were harvested, 2/5 volumes of the ice-cold "stop solution" (19% ethanol and 1% acidic phenol [pH 4.3]) was added into the cell suspension. After incubating on ice for 30 min to prevent RNA degradation (66), total RNA was extracted using TRIzol (Invitrogen, Carlsbad, CA) according to the manufacturer's protocol.

**cDNA library construction and RNA-seq.** The total RNA from the WT and  $\Delta dsrA$  strains were treated with specific biotinylated oligonucleotides to delete rRNA. A strand-specific cDNA library was constructed using Illumina TruSeq stranded mRNA kit. The obtained cDNA libraries were sequenced using Illumina HiSeq 4000 by the BGI Group (Shenzhen, Guangdong, China). After that, the adaptors were removed, and the quality of RNA-seq data was assessed using SOAP software (67). High-quality reads were mapped to the genome of *Salmonella* strain ATCC14028s using HISAT software (68). Relative expression of each individual gene was calculated by the number of fragments per kilobase of transcript per million mapped reads (FPKM) in each sample using Bowtie2 and RSEM software packages (69, 70). The DESeq2 (71) method was used to calculate the differentially expressed genes (DEGs). The genes with a fold change of  $\geq 2$  and Bonferroni-corrected *P* value ( $P_{\text{adj}}$ ) of  $< 0.05$  were determined to be DGEs.

**RT-qPCR.** Total RNA extracted from  $\text{H}_2\text{O}_2$ -treated and -untreated samples was reverse-transcribed into cDNA using the PrimeScript RT reagent kit with gDNA Eraser (TaKaRa, Dalian, China). Subsequently, the mRNA levels of the genes were determined by quantitative real-time PCR (RT-qPCR). In parallel, 16S rRNA was included as a reference for normalization of the gene expression data. Results were analyzed using the comparative critical threshold method ( $2^{-\Delta\Delta\text{CT}}$ ) (72). If the level of relative gene expression is increased or decreased by at least 2-fold, the altered expression is generally regarded as upregulation or downregulation (73).

**TABLE 1** All strains used in this study

Strain	Description	Plasmid(s)	Reference
Wild type	<i>S. Typhimurium</i> strain ATCC14028		
$\Delta dsrA$ strain	<i>dsrA</i> -deletion strain		25
$\Delta dsrA$ -pZEO strain	Negative control of $\Delta dsrA$ - <i>pdsrA</i> strain	pZEO	This study
$\Delta dsrA$ - <i>pdsrA</i> strain	The complemented strain of <i>dsrA</i>	pZEO- <i>dsrA</i>	25
$\Delta dsrA$ - <i>pdsrA</i> * strain	<i>dsrA</i> mutant ( <i>dsrA</i> *) overexpressing in $\Delta dsrA$ strain	pZEO- <i>dsrA</i> *	This study
WT-pHM1	Negative control of WT- <i>ppflB</i>	pHM1	This study
WT- <i>ppflB</i>	<i>ppflB</i> overexpressing strain	pHM- <i>ppflB</i>	This study
WT- <i>ppflB</i> - <i>pdsrA</i>	<i>ppflB</i> and <i>dsrA</i> overexpressing strain	pHM- <i>ppflB</i> , pZEO- <i>dsrA</i>	This study
pZEO- <i>phns::gfp</i>	<i>hns::gfp</i> expression fusion in $\Delta dsrA$ -pZEO strain	pXG- <i>hns::gfp</i> ; pZEO	This study
<i>pdsrA</i> - <i>phns::gfp</i>	<i>hns::gfp</i> expression fusion in $\Delta dsrA$ - <i>pdsrA</i> strain	pXG- <i>hns::gfp</i> , pZEO- <i>dsrA</i>	This study
pZEO- <i>pacnA::gfp</i>	<i>acnA::gfp</i> expression fusion in $\Delta dsrA$ -pZEO strain	pXG- <i>acnA::gfp</i>	This study
<i>pdsrA</i> - <i>pacnA::gfp</i>	<i>acnA::gfp</i> expression fusion in $\Delta dsrA$ - <i>pdsrA</i> strain	pXG- <i>acnA::gfp</i> , pZEO- <i>dsrA</i>	This study
pZEO- <i>pnuoH::gfp</i>	<i>nuoH::gfp</i> expression fusion in $\Delta dsrA$ -pZEO strain	pXG- <i>nuoH::gfp</i> ; pZEO	This study
<i>pdsrA</i> - <i>pnuoH::gfp</i>	<i>nuoH::gfp</i> expression fusion in $\Delta dsrA$ - <i>pdsrA</i> strain	pXG- <i>nuoH::gfp</i> , pZEO- <i>dsrA</i>	This study
pZEO- <i>psrLE::gfp</i>	<i>srlE::gfp</i> expression fusion in $\Delta dsrA$ -pZEO strain	pXG- <i>srlE::gfp</i> ; pZEO	This study
<i>pdsrA</i> - <i>psrLE::gfp</i>	<i>srlE::gfp</i> expression fusion in $\Delta dsrA$ - <i>pdsrA</i> strain	pXG- <i>srlE::gfp</i> , pZEO- <i>dsrA</i>	This study
pZEO- <i>ptdCB::gfp</i>	<i>tdcB::gfp</i> expression fusion in $\Delta dsrA$ -pZEO strain	pXG- <i>tdcB::gfp</i> ; pZEO	This study
<i>pdsrA</i> - <i>ptdCB::gfp</i>	<i>tdcB::gfp</i> expression fusion in $\Delta dsrA$ - <i>pdsrA</i> strain	pXG- <i>tdcB::gfp</i> , pZEO- <i>dsrA</i>	This study
pZEO- <i>pkatG::gfp</i>	<i>katG::gfp</i> expression fusion in $\Delta dsrA$ - pZEO strain	pXG- <i>katG::gfp</i> ; pZEO	This study
<i>pdsrA</i> - <i>pkatG::gfp</i>	<i>katG::gfp</i> expression fusion in $\Delta dsrA$ - <i>pdsrA</i> strain	pXG- <i>katG::gfp</i> , pZEO- <i>dsrA</i>	This study
pZEO- <i>ppflB::gfp</i>	<i>ppflB::gfp</i> expression fusion in $\Delta dsrA$ -pZEO strain	pXG- <i>ppflB::gfp</i> ; pZEO	This study
$\Delta dsrA$ - <i>pdsrA</i> - <i>ppflB::gfp</i>	<i>ppflB::gfp</i> expression fusion in $\Delta dsrA$ - <i>pdsrA</i> strain	pXG- <i>ppflB::gfp</i> , pZEO- <i>dsrA</i>	This study
$\Delta dsrA$ - <i>pdsrA</i> *- <i>ppflB::gfp</i>	<i>ppflB::gfp</i> expression fusion in $\Delta dsrA$ - <i>pdsrA</i> * strain	pXG- <i>ppflB::gfp</i> , pZEO- <i>dsrA</i> *	This study
pZEO- <i>ppflB*</i> :: <i>gfp</i>	<i>ppflB</i> mutant ( <i>ppflB</i> *) expression fusion in $\Delta dsrA$ - pZEO strain	pXG- <i>ppflB*</i> :: <i>gfp</i> ; pZEO	This study
<i>pdsrA</i> - <i>ppflB*</i> :: <i>gfp</i>	<i>ppflB</i> mutant ( <i>ppflB</i> *) expression fusion in $\Delta dsrA$ - <i>pdsrA</i> strain	pXG- <i>ppflB*</i> :: <i>gfp</i> , pZEO- <i>dsrA</i>	This study
<i>pdsrA</i> *- <i>ppflB*</i> :: <i>gfp</i>	<i>ppflB</i> mutant ( <i>ppflB</i> *) expression fusion in $\Delta dsrA$ - <i>pdsrA</i> * strain	pXG- <i>ppflB*</i> :: <i>gfp</i> , pZEO- <i>dsrA</i> *	This study
pZEO-pXG1	GFP control vector in $\Delta dsrA$ -pZEO strain	pXG1; pZEO	This study
$\Delta dsrA$ - <i>pdsrA</i> -pXG1	GFP control vector in $\Delta dsrA$ - <i>pdsrA</i> strain	pXG1; <i>pdsrA</i>	This study
$\Delta dsrA$ - <i>pdsrA</i> *-pXG1	GFP control vector in $\Delta dsrA$ - <i>pdsrA</i> * strain	pXG1; <i>pdsrA</i> *	This study
<i>rne</i> -Ctr-WT	<i>Salmonella Typhimurium</i> SL1344 ( <i>rluC-rne</i> ) IG::cat		30, 31
<i>rne</i> -TS-WT	<i>Salmonella Typhimurium</i> SL1344 ( <i>rluC-rne</i> ) IG::cat- <i>rne</i> -3071 (TS)		30, 31
<i>rne</i> -Ctr- $\Delta dsrA$	<i>dsrA</i> -deletion strain of <i>rne</i> -Ctr		This study
<i>rne</i> -Ctr- $\Delta dsrA$ -pZEO	<i>dsrA</i> -deletion strain of <i>rne</i> -Ctr harboring pZEO	pZEO	This study
<i>rne</i> -Ctr- $\Delta dsrA$ - <i>pdsrA</i>	The complemented strain of <i>dsrA</i> of <i>rne</i> -Ctr	pZEO- <i>dsrA</i>	This study
<i>rne</i> -Ctr- $\Delta dsrA$ - <i>pdsrA</i> *	<i>dsrA</i> mutant ( <i>dsrA</i> *) overexpressing in $\Delta dsrA$ strain of <i>rne</i> -Ctr	pZEO- <i>dsrA</i> *	This study
<i>rne</i> -TS- $\Delta dsrA$	<i>dsrA</i> -deletion strain of <i>rne</i> -TS		This study
<i>rne</i> -TS- $\Delta dsrA$ -pZEO	<i>dsrA</i> -deletion strain of <i>rne</i> -TS harboring pZEO	pZEO	This study
<i>rne</i> -TS- $\Delta dsrA$ - <i>pdsrA</i>	The complemented strain of <i>dsrA</i> of <i>rne</i> -TS	pZEO- <i>dsrA</i>	This study
<i>rne</i> -TS- $\Delta dsrA$ - <i>pdsrA</i> *	<i>dsrA</i> mutant ( <i>dsrA</i> *) overexpressing in $\Delta dsrA$ strain of <i>rne</i> -TS	pZEO- <i>dsrA</i> *	This study

**Construction of gene expression fusion.** A gene-*gfp* fusion was constructed as described previously (27, 28). For example, a DNA fragment containing the last 25 codons of the *focA* gene, 5' untranslated region (UTR) and CDS region of the *ppflB* gene was PCR amplified using the primer set of *ppflB*-F&R. After gel purification and NsiI/NheI digestion, the digested fragment was ligated with pXG30 for 1 h at 22°C to generate a recombinant plasmid pXG-*ppflB*. The pXG-*ppflB* plasmid was subsequently transferred into the  $\Delta dsrA$ -pZEO strain and the complemented  $\Delta dsrA$ -*pdsrA* strain, and then selected on Amp/Cm plates respectively. As a positive control, *hns::gfp* was also constructed in parallel since it is well known that DsrA represses the expression of *hns* (28). The empty plasmid pXG-1 was used as a negative control and transferred in  $\Delta dsrA$ -pZEO and  $\Delta dsrA$ -*pdsrA* strains, respectively.

**GFP fluorescence quantification.** Single colonies of the  $\Delta dsrA$  strain constructs harboring GFP fusions and DsrA expression plasmids were inoculated in triplicates into 1 mL LB broth containing Amp and Cm and grown overnight at 37°C. One hundred microliters of overnight culture was dispensed into each well of 96-well optical bottom black microtiter plates for the measurement of OD<sub>600</sub> and fluorescence (excitation at 476 nm and emission at 510 nm, using an emission cutoff filter of 495 nm) using Tecan i-control (Molecular Devices, Austria).

**Intracellular NAD<sup>+</sup>/NADH quantification.** Intracellular concentrations of NAD<sup>+</sup> and NADH in WT,  $\Delta dsrA$ ,  $\Delta dsrA$ -pZEO,  $\Delta dsrA$ -*pdsrA*, WT-pHM1, WT-*ppflB*, and WT-*ppflB*-*pdsrA* strains were measured using an NAD<sup>+</sup>/NADH cell-based assay kit (Beyotime Biotechnology, Shanghai, China). Briefly, cells treated and untreated with 3 mM H<sub>2</sub>O<sub>2</sub> for 30 min were harvested by centrifugation at 12,000 × *g* for 5 min at 4°C and resuspended in an extracting buffer to obtain the total NAD<sup>+</sup> and NADH, named NADH<sub>Total</sub>. A portion of NADH<sub>Total</sub> was heated at 60°C for 30 min to degrade NAD<sup>+</sup>. Thus, only NADH remained in the sample, named NADH<sub>NADH</sub>. The rest of NADH<sub>Total</sub> was placed at 37°C for 10 min to convert all NAD<sup>+</sup> into

NADH. Cell debris was removed from the extract by centrifugation at  $12,000 \times g$  for 10 min at  $4^{\circ}\text{C}$ . The amount of NADH in  $\text{NADH}_{\text{Total}}$  and  $\text{NADH}_{\text{NADH}}$  samples was measured separately. According to a range of NADH standards (0 to  $\sim 200$  pM), NADH concentrations in the cell extracts were determined.

**Sequence alignments.** Nucleotide sequences of the *pflB* gene from various *Salmonella* samples were downloaded from the NCBI database using the following genomes: *S. Typhimurium* 140285 (CP001363), *Salmonella enterica* serovar Typhi Ty2 (AE014613), *Salmonella enterica* serovar Enteritidis SE81 (CP050721), *Salmonella enterica* serovar Indiana JT 01 (CP028131), *Salmonella enterica* serovar Newport VNSEC031 (CP039436), *Salmonella enterica* serovar Derby CVM 30155 (CP053048), *Salmonella enterica* serovar Infantis VNSEC002 (CP039443), *Salmonella enterica* serovar Pullorum CFSAN022642 (CP075018), *Salmonella enterica* serovar Dublin USMARC-69838 (CP032449), and *Salmonella enterica* serovar Kentucky PU131 (CP026327). Alignments were generated with ClustalW software.

**Data analysis.** All the experiments were technically repeated at least three times with three biological replicates per assay. Statistical analysis of the triplicate data set was performed using the two-tailed unpaired *t* test ( $\alpha = 0.05$ ) by Microsoft Excel 2016 (Microsoft Inc., Redmond WA, USA).

**Data availability.** Gene expression data have been deposited with NCBI Gene Expression Omnibus (GEO) under accession number GSE180425.

## SUPPLEMENTAL MATERIAL

Supplemental material is available online only.

**SUPPLEMENTAL FILE 1**, PDF file, 1.2 MB.

## ACKNOWLEDGMENTS

This work was supported by the National Natural Science Foundation of China (grant no. 32172316) and the National Key R&D Program of China (grant no. 2019YFE0119700).

We thank Jörg Vogel at University of Würzburg for providing the pXG plasmid system and Chuan Wang at Fudan University for the suggestions on the target exploration and RNase E-dependent experiments.

X.S., R.D., S.H., and C.S. conceived the study and secured funding. R.D. and X.S. designed experiments. R.D. and Y.L. performed research. R.D. and Y.C. analyzed data. R.D., Y.H. and X.S. wrote the manuscript.

## REFERENCES

- Suez J, Porwollik S, Dagan A, Marzel A, Schorr YI, Desai PT, Agmon V, McClelland M, Rahav G, Gal-Mor O. 2013. Virulence gene profiling and pathogenicity characterization of non-typhoidal *Salmonella* accounted for invasive disease in humans. *PLoS One* 8:e58449. <https://doi.org/10.1371/journal.pone.0058449>.
- Haraga A, Ohlson MB, Miller SI. 2008. Salmonellae interplay with host cells. *Nat Rev Microbiol* 6:53–66. <https://doi.org/10.1038/nrmicro1788>.
- Imlay JA. 2019. Where in the world do bacteria experience oxidative stress? *Environ Microbiol* 21:521–530. <https://doi.org/10.1111/1462-2920.14445>.
- Riboulet E, Verneuil N, La Carbona S, Sauvageot N, Auffray Y, Hartke A, Giard J-C. 2007. Relationships between oxidative stress response and virulence in *Enterococcus faecalis*. *J Mol Microbiol Biotechnol* 13:140–146. <https://doi.org/10.1159/000103605>.
- Wu Y, Vulić M, Keren I, Lewis K. 2012. Role of oxidative stress in persister tolerance. *Antimicrob Agents Chemother* 56:4922–4926. <https://doi.org/10.1128/AAC.00921-12>.
- Imlay JA. 2015. Diagnosing oxidative stress in bacteria: not as easy as you might think. *Curr Opin Microbiol* 24:124–131. <https://doi.org/10.1016/j.mib.2015.01.004>.
- Imlay JA, Sethu R, Rohaun SK. 2019. Evolutionary adaptations that enable enzymes to tolerate oxidative stress. *Free Radic Biol Med* 140:4–13. <https://doi.org/10.1016/j.freeradbiomed.2019.01.048>.
- Shimizu K, Matsuoka Y. 2019. Redox rebalance against genetic perturbations and modulation of central carbon metabolism by the oxidative stress regulation. *Biotechnol Adv* 37:107441. <https://doi.org/10.1016/j.biotechadv.2019.107441>.
- Messner KR, Imlay JA. 2002. Mechanism of superoxide and hydrogen peroxide formation by fumarate reductase, succinate dehydrogenase, and aspartate oxidase. *J Biol Chem* 277:42563–42571. <https://doi.org/10.1074/jbc.M204958200>.
- Imlay JA. 2013. The molecular mechanisms and physiological consequences of oxidative stress: lessons from a model bacterium. *Nat Rev Microbiol* 11:443–454. <https://doi.org/10.1038/nrmicro3032>.
- Velali E, Pantazaki A, Besis A, Choli-Papadopoulou T, Samara C. 2019. Oxidative stress, DNA damage, and mutagenicity induced by the extractable organic matter of airborne particulates on bacterial models. *Regul Toxicol Pharmacol* 104:59–73. <https://doi.org/10.1016/j.yrtph.2019.03.004>.
- Imlay JA. 2003. Pathways of oxidative damage. *Annu Rev Microbiol* 57:395–418. <https://doi.org/10.1146/annurev.micro.57.030502.090938>.
- Nitzan M, Rehani R, Margalit H. 2017. Integration of bacterial small RNAs in regulatory networks. *Annu Rev Biophys* 46:131–148. <https://doi.org/10.1146/annurev-biophys-070816-034058>.
- Mandin P, Gottesman S. 2010. Integrating anaerobic/aerobic sensing and the general stress response through the ArcZ small RNA. *EMBO J* 29:3094–3107. <https://doi.org/10.1038/emboj.2010.179>.
- Wang L, Cai X, Wu S, Bomjan R, Nakayasu ES, Händler K, Hinton JCD, Zhou D. 2017. InvS coordinates expression of PrgH and FimZ and is required for invasion of epithelial cells by *Salmonella enterica* serovar Typhimurium. *J Bacteriol* 199:e00824-16. <https://doi.org/10.1128/JB.00824-16>.
- Xi D, Li Y, Yan J, Li Y, Wang X, Cao B. 2020. Small RNA coaR contributes to intestinal colonization in *Vibrio cholerae* via the two-component system EnvZ/OmpR. *Environ Microbiol* 22:4231–4243. <https://doi.org/10.1111/1462-2920.14906>.
- Ryan D, Ojha UK, Jaiswal S, Padhi C, Suar M. 2016. The small RNA DsrA influences the acid tolerance response and virulence of *Salmonella enterica* Serovar Typhimurium. *Front Microbiol* 7:599–607. <https://doi.org/10.3389/fmicb.2016.00599>.
- Barshishat S, Elgrably-Weiss M, Edelstein J, Georg J, Govindarajan S, Haviv M, Wright PR, Hess WR, Altuvia S. 2018. OxyS small RNA induces cell cycle arrest to allow DNA damage repair. *EMBO J* 37:413–426. <https://doi.org/10.15252/emboj.201797651>.
- Calderón IL, Morales EH, Collao B, Calderón PF, Chahuán CA, Acuña LG, Gil F, Saavedra CP. 2014. Role of *Salmonella* Typhimurium small RNAs RyhB-1 and RyhB-2 in the oxidative stress response. *Res Microbiol* 165:30–40. <https://doi.org/10.1016/j.resmic.2013.10.008>.

20. Bhatnagar K, Hinz A, Kohlman M, Wong A. 2020. An sRNA screen for reversal of quinolone resistance in *Escherichia coli*. G3 (Bethesda) 10:79–88. <https://doi.org/10.1534/g3.119.400199>.
21. Monte DF, Lincopan N, Fedorka-Cray PJ, Landgraf M. 2019. Current insights on high priority antibiotic-resistant *Salmonella enterica* in food and foodstuffs: a review. *Curr Opin Food Sci* 26:35–46. <https://doi.org/10.1016/j.cofs.2019.03.004>.
22. Storz G, Vogel J, Wassarman KM. 2011. Regulation by small RNAs in bacteria: expanding frontiers. *Mol Cell* 43:880–891. <https://doi.org/10.1016/j.molcel.2011.08.022>.
23. Beisel CL, Updegrove TB, Janson BJ, Storz G. 2012. Multiple factors dictate target selection by Hfq-binding small RNAs. *EMBO J* 31:1961–1974. <https://doi.org/10.1038/emboj.2012.52>.
24. Melamed S, Peer A, Faigenbaum-Romm R, Gatt YE, Reiss N, Bar A, Altuvia Y, Argaman L, Margalit H. 2016. Global mapping of small RNA-target interactions in bacteria. *Mol Cell* 63:884–897. <https://doi.org/10.1016/j.molcel.2016.07.026>.
25. Dong R, Qin X, He S, Zhou X, Cui Y, Shi C, He Y, Shi X. 2021. DsrA confers resistance to oxidative stress in *Salmonella enterica* serovar Typhimurium. *Food Control* 121:107571. <https://doi.org/10.1016/j.foodcont.2020.107571>.
26. Wright PR, Georg J, Mann M, Sorescu DA, Richter AS, Lott S, Kleinkauf R, Hess WR, Backofen R. 2014. CoprRNA and IntaRNA: predicting small RNA targets, networks and interaction domains. *Nucleic Acids Res* 42:W119–W123. <https://doi.org/10.1093/nar/gku359>.
27. Corcoran CP, Podkaminski D, Papenfort K, Urban JH, Hinton JCD, Vogel J. 2012. Superfolder GFP reporters validate diverse new mRNA targets of the classic porin regulator, MicF RNA. *Mol Microbiol* 84:428–445. <https://doi.org/10.1111/j.1365-2958.2012.08031.x>.
28. Urban JH, Vogel J. 2007. Translational control and target recognition by *Escherichia coli* small RNAs in vivo. *Nucleic Acids Res* 35:1018–1037. <https://doi.org/10.1093/nar/gkl1040>.
29. Chao Y, Li L, Girodat D, Förstner KU, Said N, Corcoran C, Śmiga M, Papenfort K, Reinhardt R, Wieden H-J, Luisi BF, Vogel J. 2017. In vivo cleavage map illuminates the central role of RNase E in coding and non-coding RNA pathways. *Mol Cell* 65:39–51. <https://doi.org/10.1016/j.molcel.2016.11.002>.
30. Apirion D, Lassar AB. 1978. A conditional lethal mutant of *Escherichia coli* which affects the processing of ribosomal RNA. *J Biol Chem* 253:1738–1742. [https://doi.org/10.1016/S0021-9258\(17\)34927-X](https://doi.org/10.1016/S0021-9258(17)34927-X).
31. Figueroa-Bossi N, Valentini M, Malleret L, Fiorini F, Bossi L. 2009. Caught at its own game: regulatory small RNA inactivated by an inducible transcript mimicking its target. *Genes Dev* 23:2004–2015. <https://doi.org/10.1101/gad.541609>.
32. Durica-Mitic S, Göpel Y, Görke B. 2019. Carbohydrate utilization in bacteria: making the most out of sugars with the help of small regulatory RNAs, p 229–248. In Storz G, Papenfort K (ed), *Regulating with RNA in bacteria and archaea*. American Society for Microbiology, Washington, DC.
33. Leistra AN, Curtis NC, Contreras LM. 2019. Regulatory non-coding sRNAs in bacterial metabolic pathway engineering. *Metab Eng* 52:190–214. <https://doi.org/10.1016/j.ymben.2018.11.013>.
34. Alhasawi A, Thomas SC, Appanna VD. 2016. Metabolic networks to generate pyruvate, PEP and ATP from glycerol in *Pseudomonas fluorescens*. *Enzyme Microb Technol* 85:51–56. <https://doi.org/10.1016/j.enzmictec.2016.01.007>.
35. Lemire J, Alhasawi A, Appanna VP, Tharmalingam S, Appanna VD. 2017. Metabolic defence against oxidative stress: the road less travelled so far. *J Appl Microbiol* 123:798–809. <https://doi.org/10.1111/jam.13509>.
36. Grüning N-M, Rinnerthaler M, Bluemlein K, Müllereder M, Wamelink MMC, Lehrach H, Jakobs C, Breitenbach M, Ralsler M. 2011. Pyruvate kinase triggers a metabolic feedback loop that controls redox metabolism in respiring cells. *Cell Metab* 14:415–427. <https://doi.org/10.1016/j.cmet.2011.06.017>.
37. Rui B, Shen T, Zhou H, Liu J, Chen J, Pan X, Liu H, Wu J, Zheng H, Shi Y. 2010. A systematic investigation of *Escherichia coli* central carbon metabolism in response to superoxide stress. *BMC Syst Biol* 4:122. <https://doi.org/10.1186/1752-0509-4-122>.
38. Lemire J, Milandu Y, Auger C, Bignucolo A, Appanna VP, Appanna VD. 2010. Histidine is a source of the antioxidant,  $\alpha$ -ketoglutarate, in *Pseudomonas fluorescens* challenged by oxidative stress. *FEMS Microbiol Lett* 309:170–177. <https://doi.org/10.1111/j.1574-6968.2010.02034.x>.
39. Fröhlich KS, Haneke K, Papenfort K, Vogel J. 2016. The target spectrum of SdsR small RNA in *Salmonella*. *Nucleic Acids Res* 44:10406–10422. <https://doi.org/10.1093/nar/gkw632>.
40. Iosub IA, van Nues RW, McKellar SW, Nieken KJ, Marchioretto M, Sy B, Tree JJ, Viero G, Granneman S. 2020. Hfq CLASH uncovers sRNA-target interaction networks linked to nutrient availability adaptation. *Elife* 9:e54655. <https://doi.org/10.7554/eLife.54655>.
41. Melamed S, Adams PP, Zhang A, Zhang H, Storz G. 2020. RNA-RNA interactomes of ProQ and Hfq reveal overlapping and competing roles. *Mol Cell* 77:411–425. <https://doi.org/10.1016/j.molcel.2019.10.022>.
42. Barquist L, Vogel J. 2015. Accelerating discovery and functional analysis of small RNAs with new technologies. *Annu Rev Genet* 49:367–394. <https://doi.org/10.1146/annurev-genet-112414-054804>.
43. Kröger C, Colgan A, Srikanth S, Händler K, Sivasankaran SK, Hammarlöf DL, Canals R, Grissom JE, Conway T, Hokamp K, Hinton JCD. 2013. An infection-relevant transcriptomic compendium for *Salmonella enterica* serovar Typhimurium. *Cell Host Microbe* 14:683–695. <https://doi.org/10.1016/j.chom.2013.11.010>.
44. Wu P, Liu X, Yang L, Sun Y, Gong Q, Wu J, Shi Y. 2017. The important conformational plasticity of DsrA sRNA for adapting multiple target regulation. *Nucleic Acids Res* 45:9625–9639. <https://doi.org/10.1093/nar/gkx570>.
45. Cayrol B, Fortas E, Martret C, Cech G, Kloska A, Caulet S, Barbet M, Trépout S, Marco S, Taghbalout A, Busi F, Wegrzyn G, Arluison V. 2015. Riboregulation of the bacterial actin-homolog MreB by DsrA small noncoding RNA. *Integr Biol (Camb)* 7:128–141. <https://doi.org/10.1039/c4ib00102h>.
46. McCullen CA, Benhammou JN, Majdalani N, Gottesman S. 2010. Mechanism of positive regulation by DsrA and RprA small noncoding RNAs: pairing increases translation and protects rpoS mRNA from degradation. *J Bacteriol* 192:5559–5571. <https://doi.org/10.1128/JB.00464-10>.
47. Lalaouna D, Morissette A, Carrier M-C, Massé E. 2015. DsrA regulatory RNA represses both *hns* and *rbsD* mRNAs through distinct mechanisms in *Escherichia coli*. *Mol Microbiol* 98:357–369. <https://doi.org/10.1111/mmi.13129>.
48. Lee H-J, Gottesman S. 2016. sRNA roles in regulating transcriptional regulators: Lrp and SoxS regulation by sRNAs. *Nucleic Acids Res* 44:6907–6923. <https://doi.org/10.1093/nar/gkw358>.
49. Prévost K, Desnoyers G, Jacques J-F, Lavoie F, Massé E. 2011. Small RNA-induced mRNA degradation achieved through both translation block and activated cleavage. *Genes Dev* 25:385–396. <https://doi.org/10.1101/gad.200171>.
50. Lalaouna D, Eyraud A, Devinck A, Prévost K, Massé E. 2019. GcvB small RNA uses two distinct seed regions to regulate an extensive targetome. *Mol Microbiol* 111:473–486. <https://doi.org/10.1111/mmi.14168>.
51. Morita T, Maki K, Aiba H. 2005. RNase E-based ribonucleoprotein complexes: mechanical basis of mRNA destabilization mediated by bacterial noncoding RNAs. *Genes Dev* 19:2176–2186. <https://doi.org/10.1101/gad.1330405>.
52. Pfeiffer V, Papenfort K, Lucchini S, Hinton JCD, Vogel J. 2009. Coding sequence targeting by MicC RNA reveals bacterial mRNA silencing downstream of translational initiation. *Nat Struct Mol Biol* 16:840–846. <https://doi.org/10.1038/nsmb.1631>.
53. Del Campo C, Bartholomäus A, Fedyunin I, Ignatova Z. 2015. Secondary structure across the bacterial transcriptome reveals versatile roles in mRNA regulation and function. *PLoS Genet* 11:e1005613. <https://doi.org/10.1371/journal.pgen.1005613>.
54. Moll I, Afonyushkin T, Vytvytska O, Kaberdin VR, Bläsi U. 2003. Coincident Hfq binding and RNase E cleavage sites on mRNA and small regulatory RNAs. *RNA* 9:1308–1314. <https://doi.org/10.1261/ma.5850703>.
55. Bandyra KJ, Said N, Pfeiffer V, Górna MW, Vogel J, Luisi BF. 2012. The seed region of a small RNA drives the controlled destruction of the target mRNA by the endoribonuclease RNase E. *Mol Cell* 47:943–953. <https://doi.org/10.1016/j.molcel.2012.07.015>.
56. Link TM, Valentin-Hansen P, Brennan RG. 2009. Structure of *Escherichia coli* Hfq bound to polyribadenylate RNA. *Proc Natl Acad Sci U S A* 106:19292–19297. <https://doi.org/10.1073/pnas.0908744106>.
57. Robinson KE, Orans J, Kovach AR, Link TM, Brennan RG. 2014. Mapping Hfq-RNA interaction surfaces using tryptophan fluorescence quenching. *Nucleic Acids Res* 42:2736–2749. <https://doi.org/10.1093/nar/gkt1171>.
58. Miyakoshi M, Matera G, Maki K, Sone Y, Vogel J. 2019. Functional expansion of a TCA cycle operon mRNA by a 3' end-derived small RNA. *Nucleic Acids Res* 47:2075–2088. <https://doi.org/10.1093/nar/gky1243>.
59. Sawers RG. 2006. Differential turnover of the multiple processed transcripts of the *Escherichia coli* *focA-pflB* operon. *Microbiology (Reading)* 152:2197–2205. <https://doi.org/10.1099/mic.0.28951-0>.

60. Causey TB, Shanmugam KT, Yomano LP, Ingram LO. 2004. Engineering *Escherichia coli* for efficient conversion of glucose to pyruvate. *Proc Natl Acad Sci U S A* 101:2235–2240. <https://doi.org/10.1073/pnas.0308171100>.
61. Jian X, Li N, Zhang C, Hua Q. 2016. In silico profiling of cell growth and succinate production in *Escherichia coli* NZN111. *Bioresour Bioprocess* 3: 48. <https://doi.org/10.1186/s40643-016-0125-5>.
62. Zhang X, Shanmugam KT, Ingram LO. 2010. Fermentation of glycerol to succinate by metabolically engineered strains of *Escherichia coli*. *Appl Environ Microbiol* 76:2397–2401. <https://doi.org/10.1128/AEM.02902-09>.
63. Kessler D, Herth W, Knappe J. 1992. Ultrastructure and pyruvate formate-lyase radical quenching property of the multienzymic AdhE protein of *Escherichia coli*. *J Biol Chem* 267:18073–18079. [https://doi.org/10.1016/S0021-9258\(19\)37154-6](https://doi.org/10.1016/S0021-9258(19)37154-6).
64. Datsenko KA, Wanner BL. 2000. One-step inactivation of chromosomal genes in *Escherichia coli* K-12 using PCR products. *Proc Natl Acad Sci U S A* 97:6640–6645. <https://doi.org/10.1073/pnas.120163297>.
65. Wang C, Chao Y, Matera G, Gao Q, Vogel J. 2020. The conserved 3' UTR-derived small RNA NarS mediates mRNA crossregulation during nitrate respiration. *Nucleic Acids Res* 48:2126–2143. <https://doi.org/10.1093/nar/gkz1168>.
66. Tedin K, Bläsi U. 1996. The RNA chain elongation rate of the  $\lambda$  Late mRNA is unaffected by high levels of ppGpp in the absence of amino acid starvation. *J Biol Chem* 271:17675–17686. <https://doi.org/10.1074/jbc.271.30.17675>.
67. Li R, Li Y, Kristiansen K, Wang J. 2008. SOAP: short oligonucleotide alignment program. *Bioinformatics* 24:713–714. <https://doi.org/10.1093/bioinformatics/btn025>.
68. Kim D, Langmead B, Salzberg SL. 2015. HISAT: a fast spliced aligner with low memory requirements. *Nat Methods* 12:357–360. <https://doi.org/10.1038/nmeth.3317>.
69. Li B, Dewey CN. 2011. RSEM: accurate transcript quantification from RNA-Seq data with or without a reference genome. *BMC Bioinformatics* 12: 323. <https://doi.org/10.1186/1471-2105-12-323>.
70. Langmead B, Salzberg SL. 2012. Fast gapped-read alignment with Bowtie 2. *Nat Methods* 9:357–359. <https://doi.org/10.1038/nmeth.1923>.
71. Love MI, Huber W, Anders S. 2014. Moderated estimation of fold change and dispersion for RNA-seq data with DESeq2. *Genome Biol* 15:550. <https://doi.org/10.1186/s13059-014-0550-8>.
72. Livak KJ, Schmittgen TD. 2001. Analysis of relative gene expression data using real-time quantitative PCR and the  $2^{-\Delta\Delta CT}$  method. *Methods* 25: 402–408. <https://doi.org/10.1006/meth.2001.1262>.
73. Desroche N, Beltramo C, Guzzo J. 2005. Determination of an internal control to apply reverse transcription quantitative PCR to study stress response in the lactic acid bacterium *Oenococcus oeni*. *J Microbiol Methods* 60:325–333. <https://doi.org/10.1016/j.mimet.2004.10.010>.